Supporting information for

On-site portable detection of gaseous methyl iodide using electrochemical method

Xiao-Lan Yang, Qiu-Hong Zhu, Guo-Hao Zhang, Jie Fu, Shuang-Long Wang, Lijian Ma, Song Qin, Guo-Hong Tao*, Ling He*

College of Chemistry, Sichuan University, Chengdu, Sichuan 610064, China.

E-mail: lhe@scu.edu.cn.

E-mail: taogh@scu.edu.cn.

Table of Contents

Experimental Section

Materials

In this work, the chemicals used for the preparation of PVIm were 1-vinylimidazole (VIm, 98%) monomer and azobisisobutyronitrile (AIBN) initiator, both of which were obtained from Energy Chemical and used as received. Polyvinylpyrrolidone (PVP), poly(4-vinylpyridine-co-styrene) (P(4VP-St)) and poly ethyleneimine (PEI, 99%) for polarity comparison were purchased from Leyan and Energy Chemical. Methyl iodide (CH_3I, 99%) used for the detection was obtained from Xiya reagents. All other analytical grade chemicals and reagents were got commercially and used without further purification. Ultrapure water of 18.25 MΩ.cm was used throughout the experiment.

Synthesis of $PVIm_x$ (x = 0.01, 0.03, 0.05, 0.10)

PVIm homopolymers were prepared by the free radical polymerization reaction of VIm in dimethyl sulfoxide (DMSO) solution with AIBN as the free radical initiator. The molecular weight of PVIm was controlled by changing the masses of AIBN.

Scheme S1. The synthesis route of PVIm.

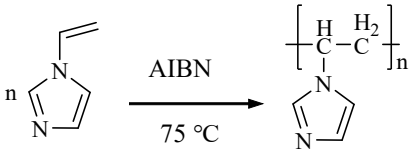

PVIm was synthesized by the similar method described in the literature [1]. First, 4.0816 mL VIm, 12 mL DMSO and different masses of AIBN (1 wt%, 3 wt%, 5 wt% and 10 wt% of VIm, respectively) were mixed in the pressure pipes. After freeze-drying, polymerization was carried out at 75 °C for 12 h. And then, cooled the obtained yellow viscous solution to room temperature, precipitated twice in ethyl acetate (EA)

and filtered. Finally, a light yellow solid was obtained after vacuum drying filter cake at 60 °C for 48 hours. The synthesized samples were named as $PVIm_{0.01}$, $PVIm_{0.03}$, $PVIm_{0.05}$ and $PVIm_{0.10}$ with the yields of 77.3%, 81.1%, 84.5% and 90.8%.

The ^{1}H signal peaks at 1.6-2.2 ppm are attributed to the protons of CH_2 (H1) on the main chain. Peaks at 2.4-3.2 ppm are assigned to protons on the CH (H2) group of the polymer backbone for the syndiotactic, heterotactic, and aisotactic triads[2]. The protons (H3, H4, and H5) of the imidazole ring occur at 6.6-7.4 ppm. The imidazole ring carbons of C3, C4 and C5 are observed at 116.5-136.9 ppm. The CH_2 and CH carbons on the main chain appear at 50.9-52.9 ppm and 38.9-41.6 ppm, respectively.

Synthesis of $PVIm_x$-F (x = 0.01, 0.03, 0.05, 0.10)

The $PVIm_x$ films were prepared in the following manners. Dissolved a certain amount of $PVIm_x$ in ethanol (EtOH), and then the solution was poured into molds to form films by solvent evaporation. The as-prepared $PVIm_x$ films were named $PVIm_{0.01}$-F, $PVIm_{0.03}$-F, $PVIm_{0.05}$-F and $PVIm_{0.10}$-F.

Material characterization

NMR spectra of $PVIm_x$ homopolymers were recorded by a Bruker 400 MHz nuclear magnetic resonance (NMR) spectrometer (Germany). The chemical shifts were reported in ppm relative to TMS. The ^{1}H NMR of $PVIm_x$ was probed with DMSO d_6 as the locking solvent. Because of the large molecular weight of $PVIm_x$ and their limited solubility in the regulated DMSO d_6, we chose the good solvent methanol-d_4 for the ^{13}C NMR analysis. Fourier transform infrared (FT-IR) spectra in the range of 400-4000 cm^{-1} were recorded using a Bruker ALPHA (Germany) infrared spectrometer. Gel Permeation Chromatography (GPC, waters1525 & Agilent PL-220) was used to measure the weight-average molecular weight of the four polymers. The transmittances of $PVIm_x$-F were characterized by scanning the wavelength 400 to 800 nm using an ultraviolet visible spectrophotometer (Rayleigh UV-1601). The powder X-ray

diffraction (PXRD) instrument (Schimadzu-XRD-6100, Japan) and polarization optical microscope (POM) were used to check the crystallinity of $PVIm_x$-F. Contact angle (CA) images were recorded on the ZHONGCHEN JC2000DS (China) contact angle measuring instrument equipped with a CCD camera. Digital photographs of $PVIm_x$-F were recorded with a Redmi K40, SEM and energy-dispersive spectrometry (EDS) imaging was performed with JSM-7500F (Japan) and TM3000 scanning electron microscopes. For thermal properties, the glass transition temperatures (T_g) of the samples were determined by a TA Q20 differential scanning calorimeter (DSC) at a nitrogen flow rate of 50 mL/min and a scan rate of 10 °C/min, where an empty aluminum container was the reference sample. And the decomposition temperature (T_d) of the samples was determined by a thermogravimetric analysis (TGA, NETZSCH TG209F1), where the tests were performed at 10 °C/min from ambient temperature to 600 °C. The structures of the samples were analyzed by X-ray photoelectron spectroscopy (XPS, Thermo Scientific K-Alpha+). The zeta potential of the films at 298 k were determined by Zetasizer Nano ZS90 DLS spectrometer (Malvern Inc., UK), and the pH of the systems were controlled between 3-11 by 0.01 mol/L NaOH and 0.01 mol/L HCl solutions.

Electrochemical tests

The ionic conductivities (σ) of the samples were measured by EIS on an Autolab M204 electrochemical workstation. The effective areas of all $PVIm_x$-F samples in this work were controlled at 1 × 1 cm^2 with a frequency range of 0.1 Hz-10^6 Hz and an amplitude of 10 mV. The $PVIm_x$-F film were sandwiched between a pair of stainless steel electrodes, and the σ was calculated by the following equation:

$$\sigma = \frac{L}{RS}$$

where R is the bulk resistance (Ω) of PVIm-F measured by the EIS method, L is the thickness of PVIm-F (cm), and S is the effective area of the PVIm-F film (cm^2).

To be specific, CH_3I and a $PVIm_x$-F were placed in a 15 L closed container, and

then heated CH_3I at 50 °C to vaporize. When the system is stable, allowing it to contact PVIm-F 20 min and undergo a quaternization reaction. Without special instructions, each EIS was tested 5 times in parallel at a relative humidity of 50%.

Theoretical calculations

Based on the density functional theory (DFT) method and the Gaussian 09 (Revision A.02) suite of programs[3], the dimer model of PVIm and the other corresponding compounds were subjected to structural optimization and natural bond orbital (NBO) calculation in the gas phase at the B3LYP-D3/6-311g(d,P) level and B3LYP-D3/def2TZVP level, respectively. The frequency calculations for all structurally optimized compounds showed no imaginary frequencies, indicating that their geometric energies were at the minimum value. GaussView 5.0 was used to view the energy level energies and orbit images of all optimized compounds.

Results and Discussion

Fig. S1. The ^{1}H NMR spectrum of $PVIm_{0.01}$.

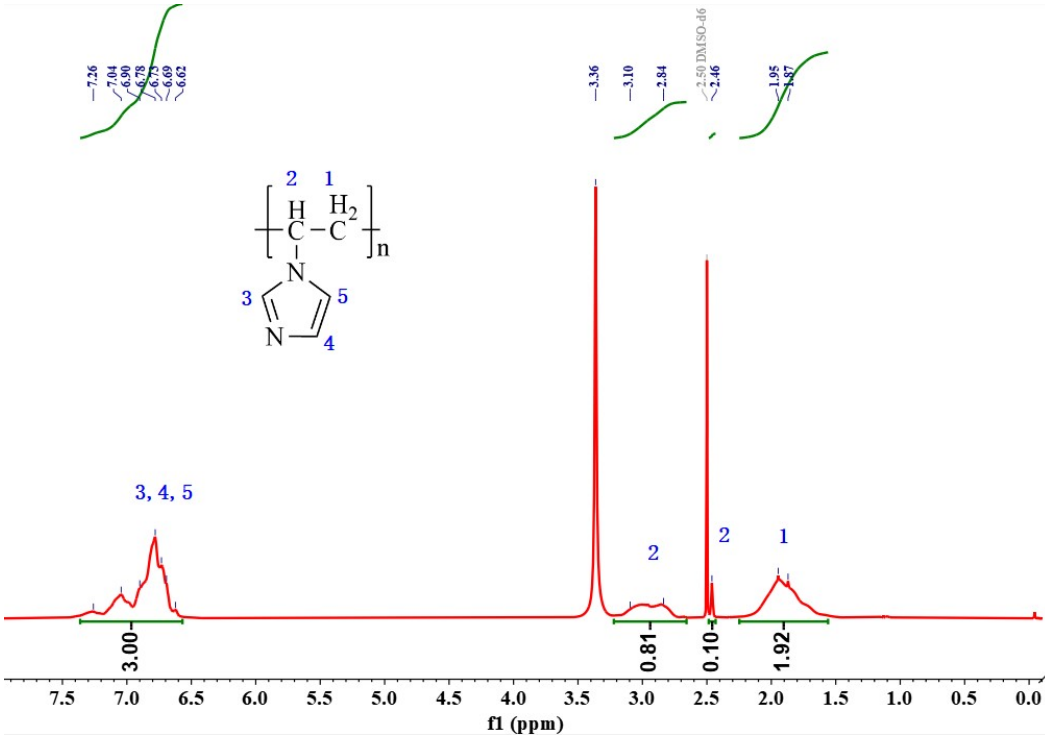

Fig. S2. The ^{1}H NMR spectrum of $PVIm_{0.03}$.

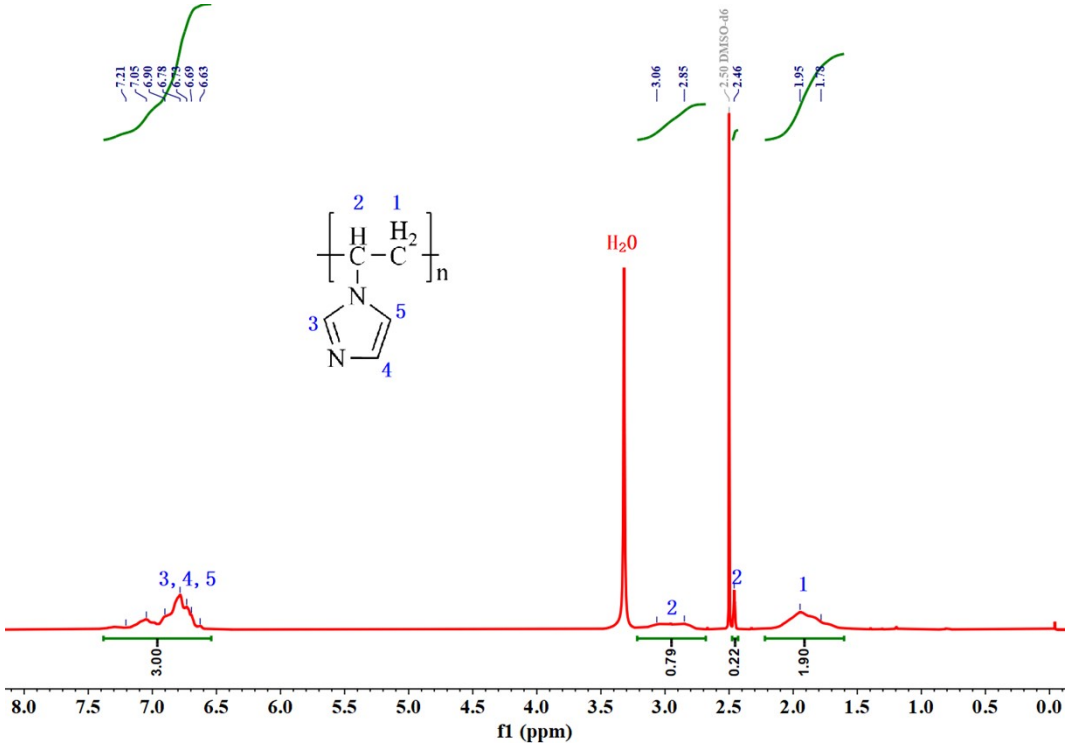

Fig. S3. The ^{1}H NMR spectrum of $PVIm_{0.05}$.

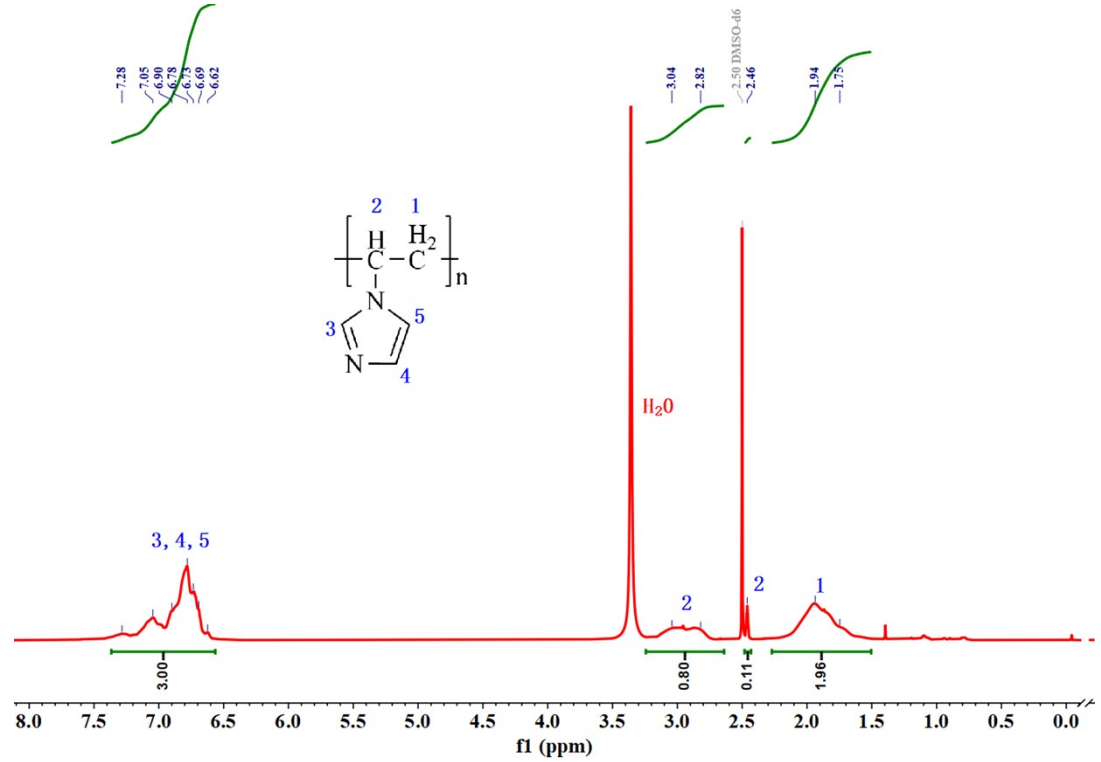

Fig. S4. The ^{1}H NMR spectrum of $PVIm_{0.10}$.

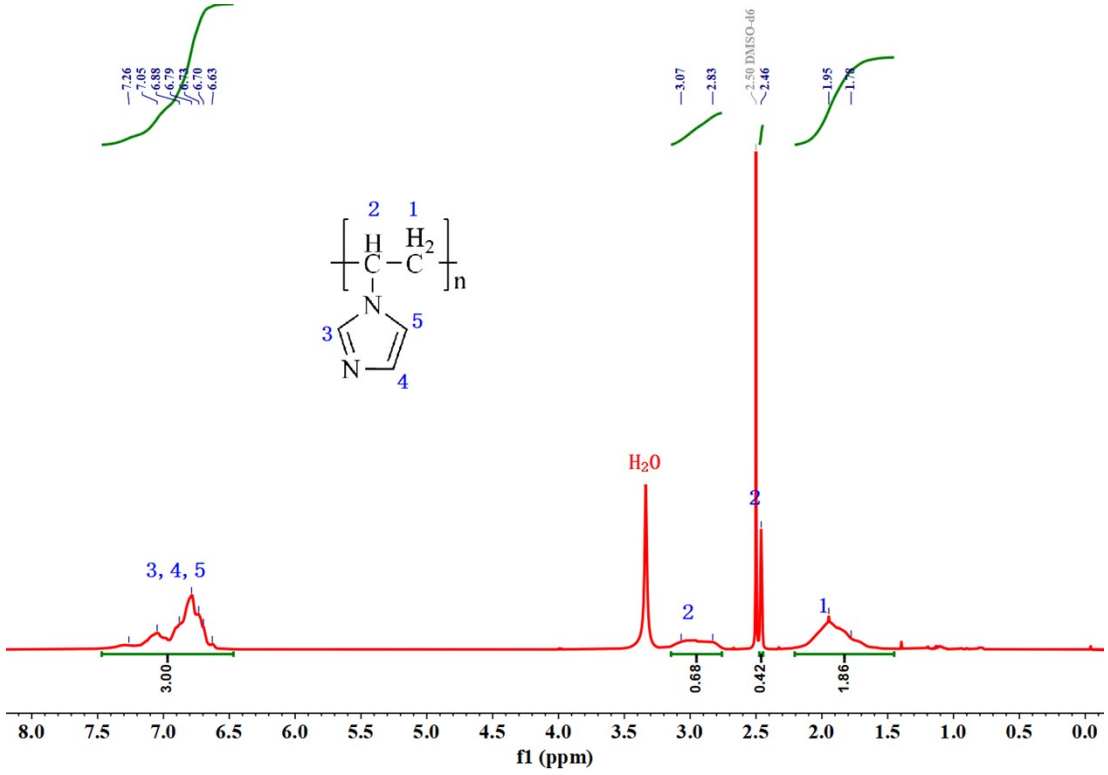

Fig. S5. The ^{13}C NMR spectrum of $PVIm_{0.01}$.

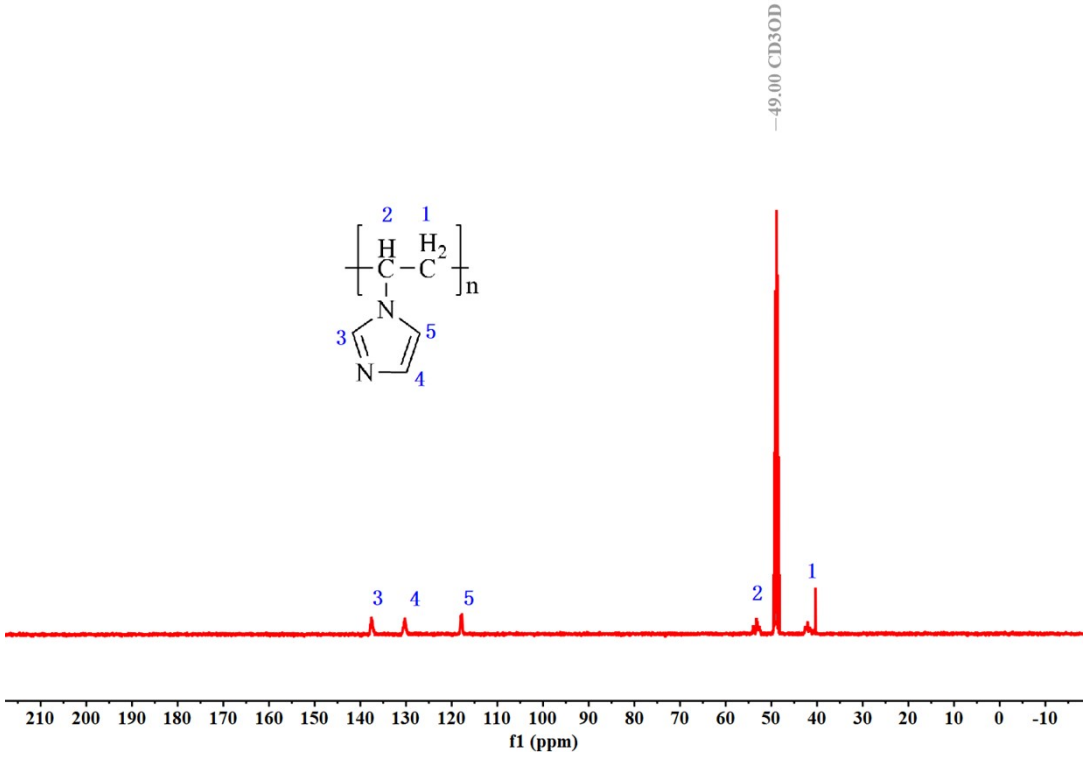

Fig. S6. The ^{13}C NMR spectrum of $PVIm_{0.03}$.

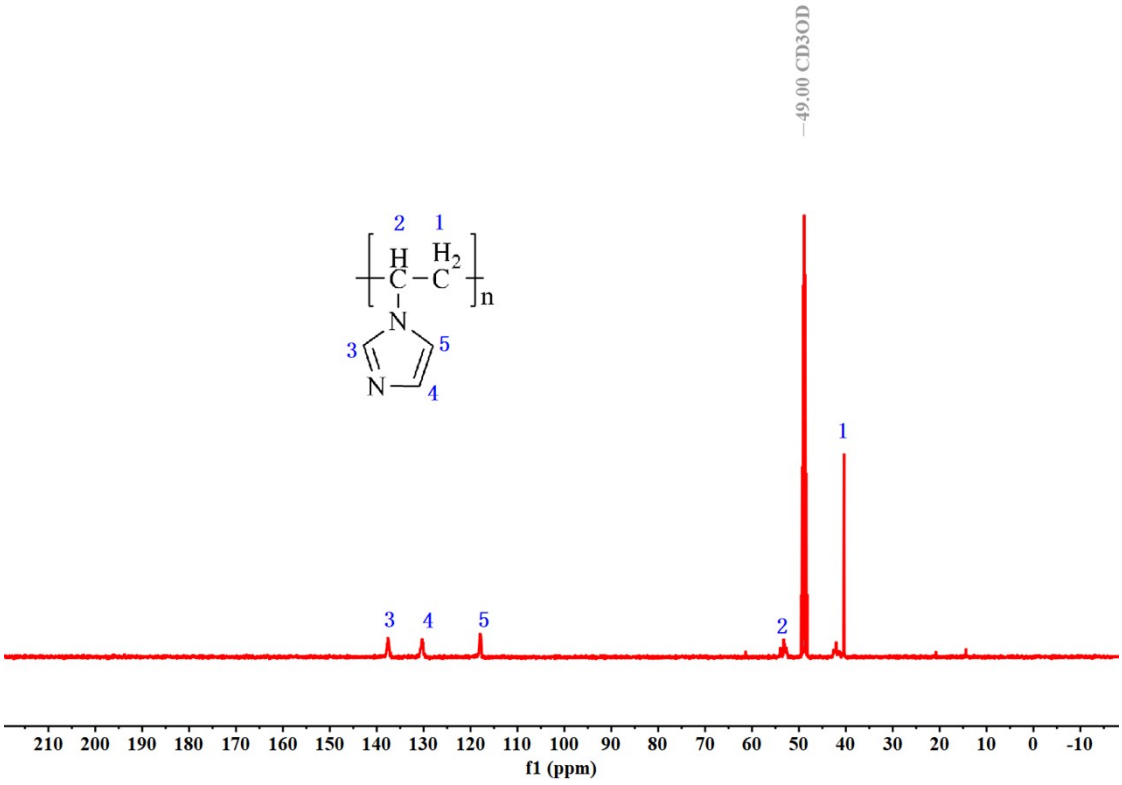

Fig. S7. The ^{13}C NMR spectrum of $PVIm_{0.05}$.

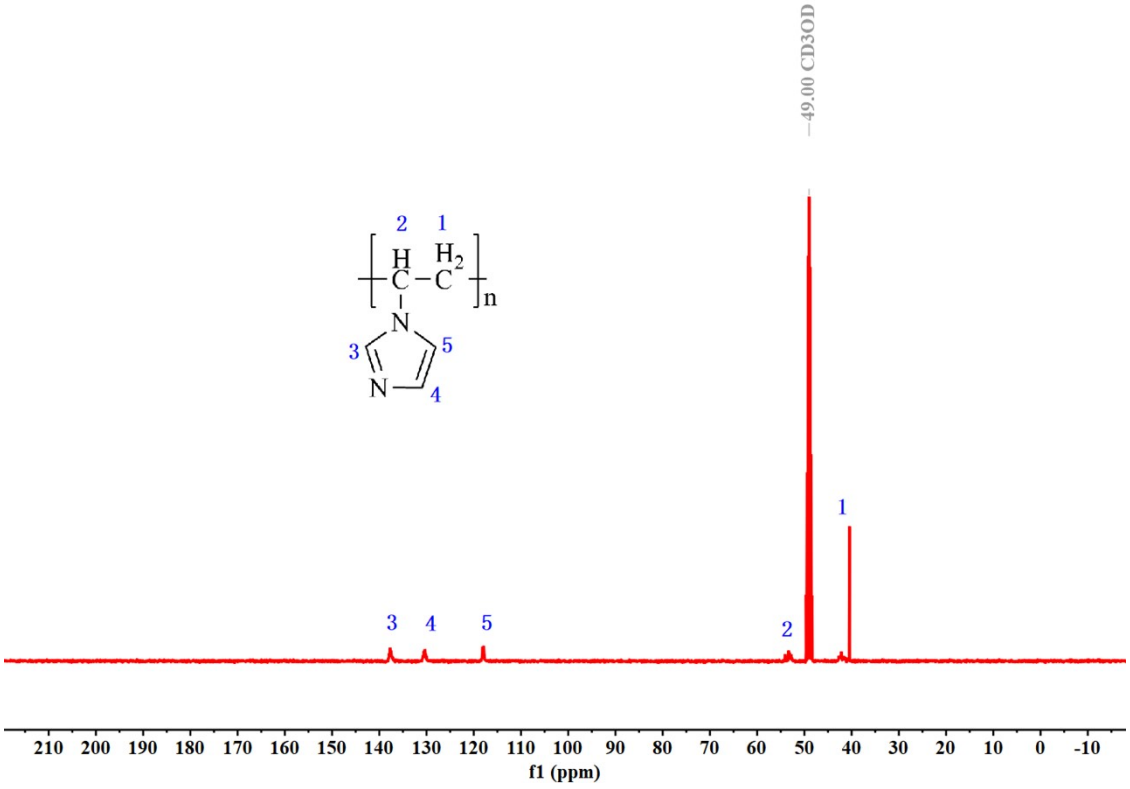

Fig. S8. The ^{13}C NMR spectrum of $PVIm_{0.10}$.

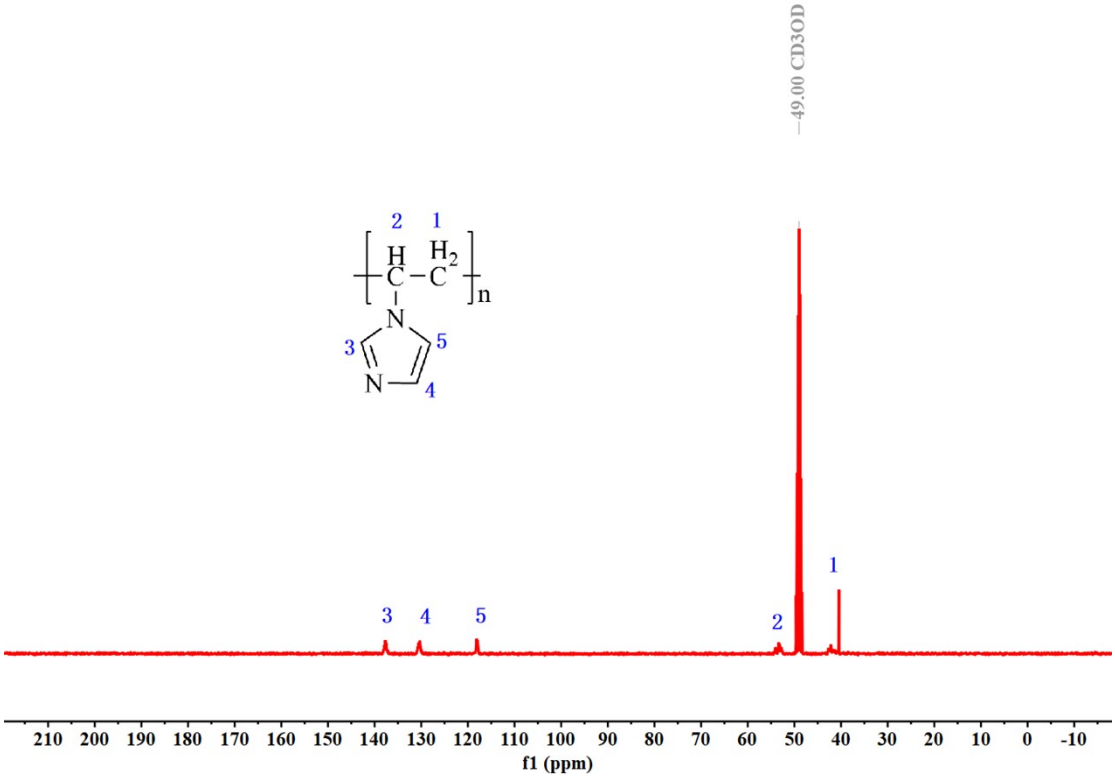

Fig. S9. The FT-IR spectra of VIm and $PVIm_x$.

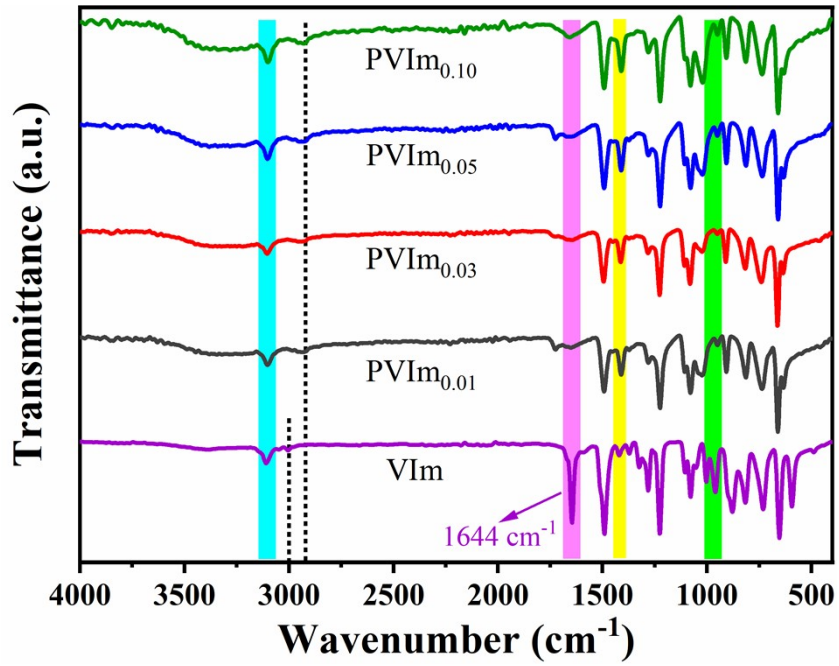

Table S1. Molecular weight analysis of $PVIm_x$.

	peak	Mn	Mw	Mp	Mz	Mz+1	Polydispersity	Mz/Mw	Mz+1/Mw
$PVIm_{0.01}$	1	28406	69859	60681	127939	191908	2.459306	1.831394	2.747089
$PVIm_{0.03}$	2	23244	59575	52015	111351	171239	2.563016	1.869090	2.874346
$PVIm_{0.05}$	3	16256	45045	42074	82580	120478	2.771265	1.833103	2.674358
$PVIm_{0.10}$	4	16818	44279	39588	83005	125103	2.632798	1.874594	2.825335

Fig. S10. Equivalent circuit diagram.

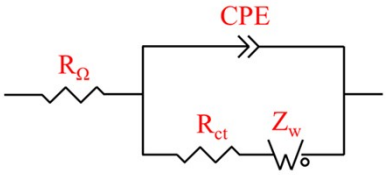

Fig. S11. EIS plots of $PVIm_{0.01}$-F with different thicknesses after the reaction with (a) 0 and (b) 1000 ppm of CH_3I.

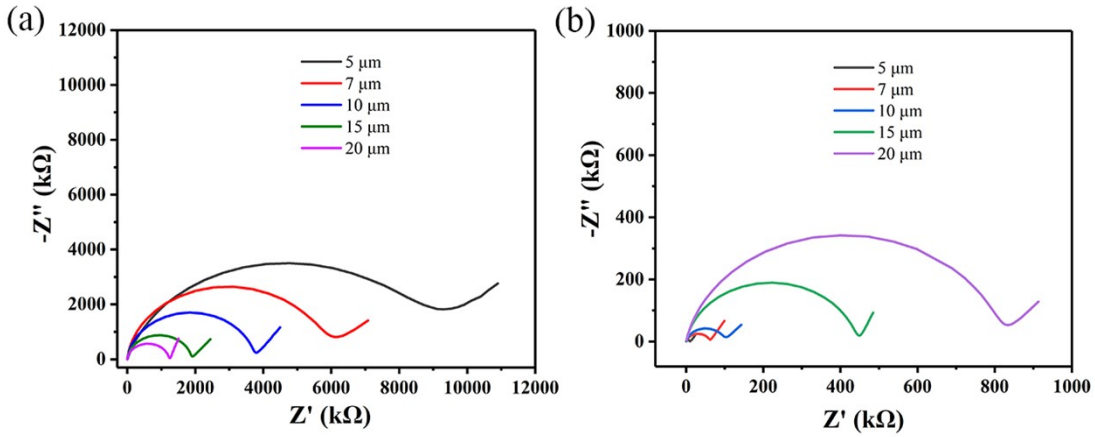

Fig. S12. Effect of film thickness on $PVIm_{0.01}$-F impedance on σ at CH_3I concentrations of 0 and 1000 ppm.

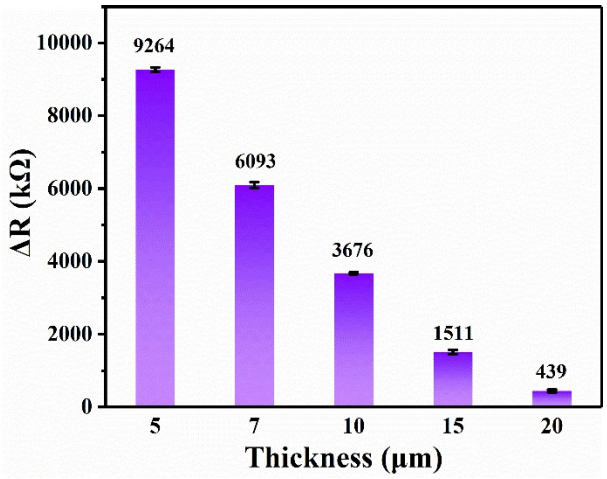

Fig. S13. EIS plots of $PVIm_x$-F after the reaction with (a) 0 and (b)1000 ppm of CH_3I.

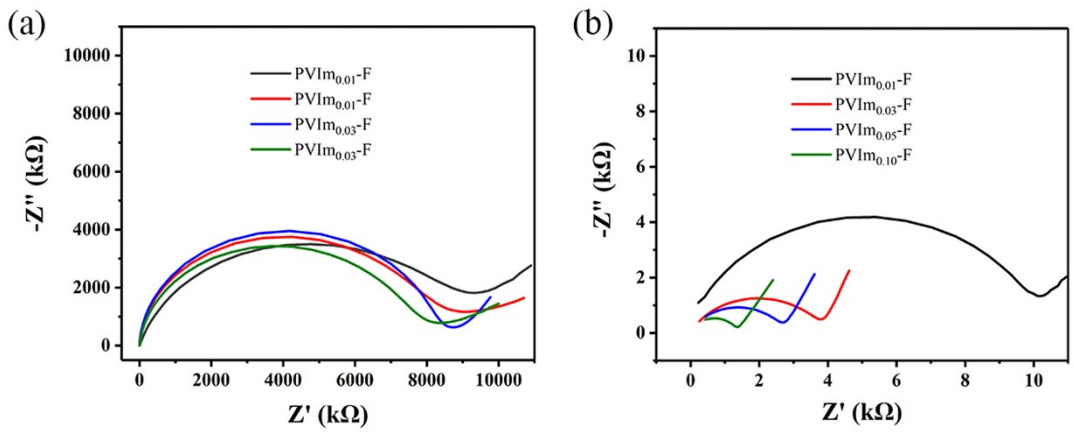

Fig. S14. Effect of film types on σ for the same thickness at CH_3I concentrations of 0 and 1000 ppm.

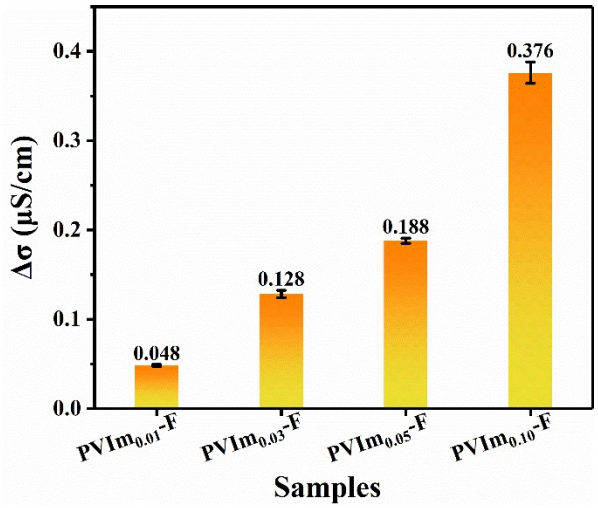

Fig. S15. (a) EIS and (b) σ graphs of $PVIm_{0.10}$-F after the reaction with 60 ppm CH_3I at different RH levels.

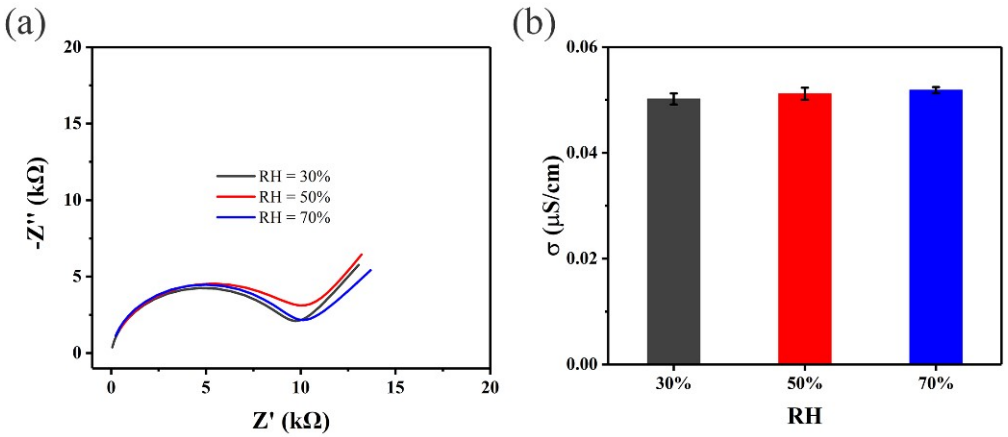

Table S2. Summary of detection limits previously reported in this field.

Serial no.	Sensor/Product	Detection method	Time	LOD	Ref.
1	Sol-gel	Colorimetric method	14 h	3 mg/L	[4]
2	NBP/N6NFM	Colorimetric method	5 min	0.5 ppm	[5]
3	NBP/DEAE@N6 NFM	Colorimetric method	5 min	0.1 ppm	[6]
4	$PVIm_{0.10}$-F	EIS	20 min	0.474 ppb	This work

Table S3. The cost of the currently reported CH_3I detection materials and the price of some disposable consumables.

Serial no.	Sensor/Product	Costing/Price	Ref.
1	$PbCsBr_3$	440 ¢/g	[7]
2	NBP/DEAE@N6NFM	370 ¢/g	[6]
3	pyridine 1	29 ¢/g	[8]
4	Starch iodine paper	0.36 ¢/strip	-
5	$PVIm_{0.10}$-F	0.10 ¢/piece or 8 ¢/g	This work
6	pH test paper	0.08 ¢/strip	-

Table S4. HOMO-LOMO orbital energy calculation.

	Orbital energy (eV)	Orbital energy difference (eV)	Orbital diagram
PVIm (HOMO)	-6.397	——	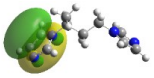
O_2 (LOMO)	-5.134	1.263	
I_2 (LOMO)	-3.948	2.449	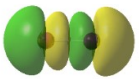
Cl_2 (LOMO)	-3.529	2.868	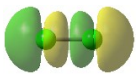
CH_3I (LOMO)	-1.151	5.246	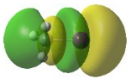
N_2 (LOMO)	-0.822	5.575	
CO_2 (LOMO)	0.362	6.759	
H_2O (LOMO)	0.374	6.771	
NH_3 (LOMO)	0.639	7. 036	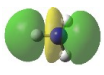
CH_4 (LOMO)	1.304	7.701	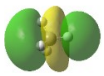
H_2 (LOMO)	1.569	7.966	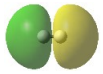

Fig. S16. The electrochemical response of $PVIm_{0.10}$-F to 50 ppm CH_3I and other organic halides under dynamic air flow simulation, (a) EIS and (b) conductivity chart.

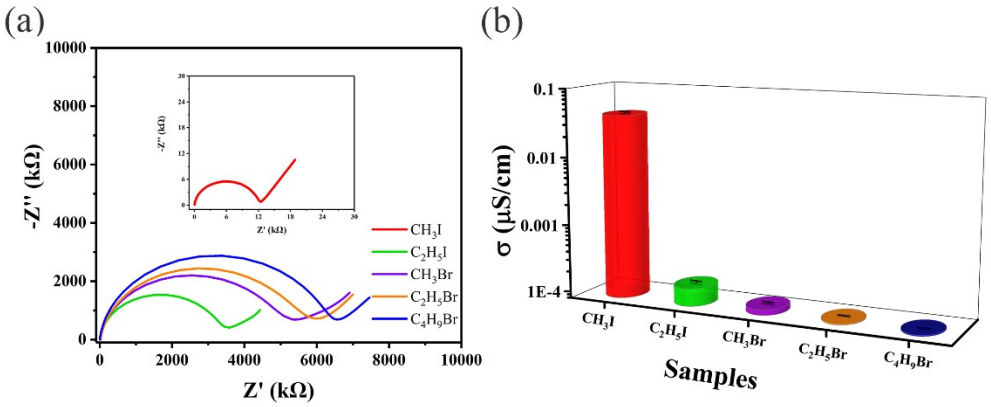

Fig. S17. FT-IR analysis of $PVIm_x$-F after the reaction with CH_3I.

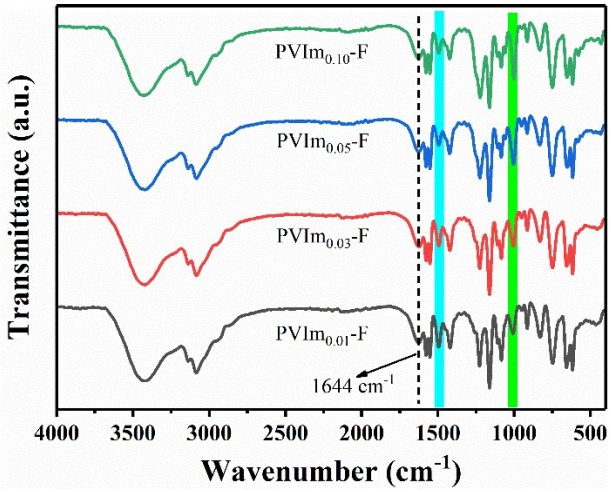

Fig. S18. Full survey XPS spectra of $PVIm_{0.10}$-F before and after the reaction with CH_3I.

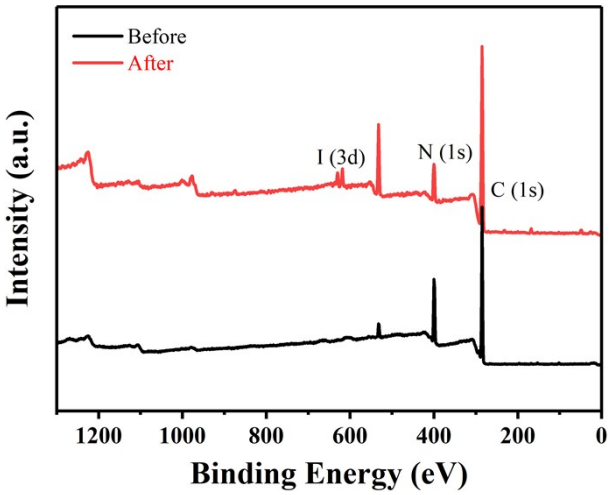

Fig. S19. I 3d XPS spectra of $PVIm_{0.10}$-F before and after the reaction with CH_3I.

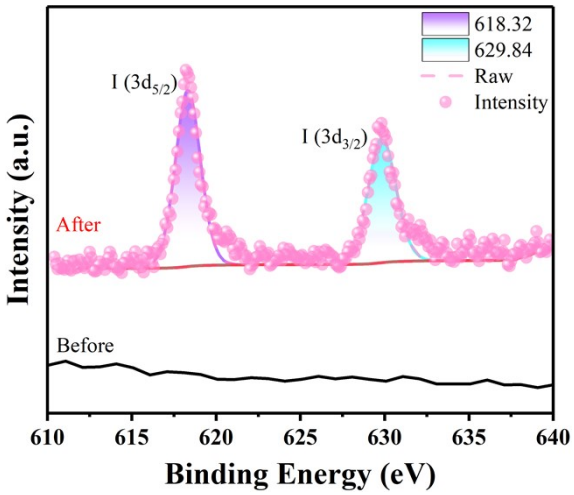

Fig. S20. EDX of $PVIm_x$-F after the reaction with CH_3I.

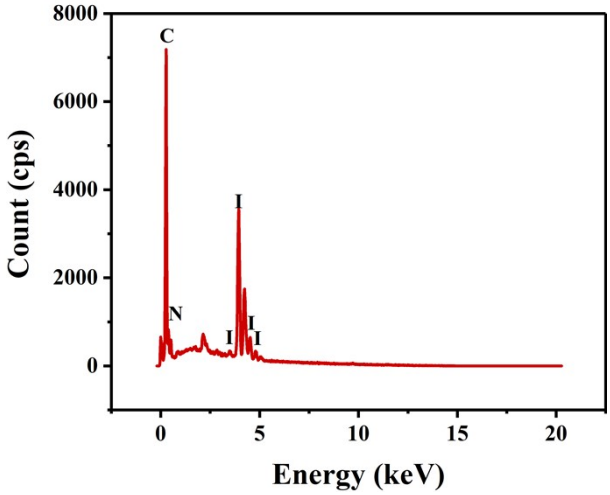

Fig. S21. Time-dependent contact angles of $PVIm_x$-F before the reaction with CH_3I.

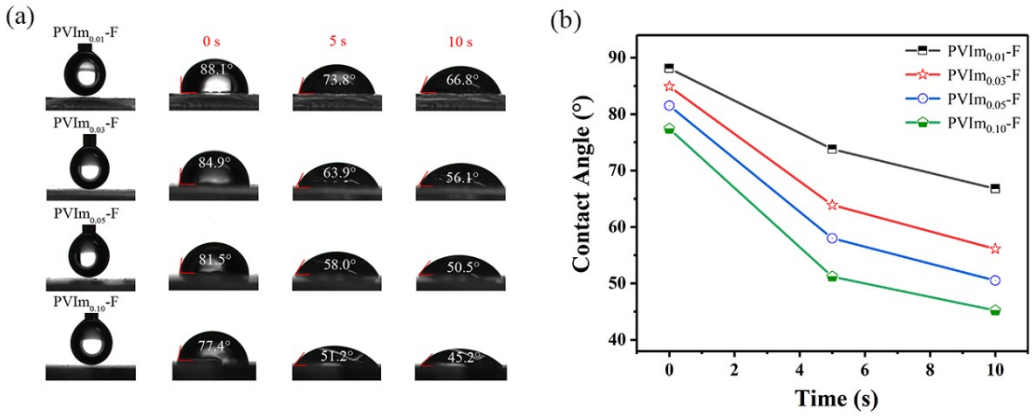

Fig. S22. Time-dependent contact angles of $PVIm_x$-F after the reaction with CH_3I.

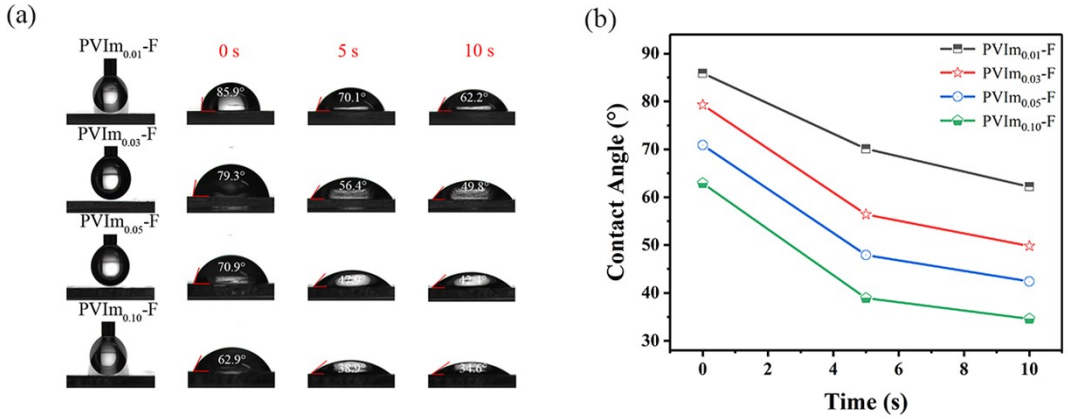

Fig. S23. (a) EIS stability of sensors after storage for different times. (b) EIS signal response of devices at different time points to 40 ppm CH_3I.

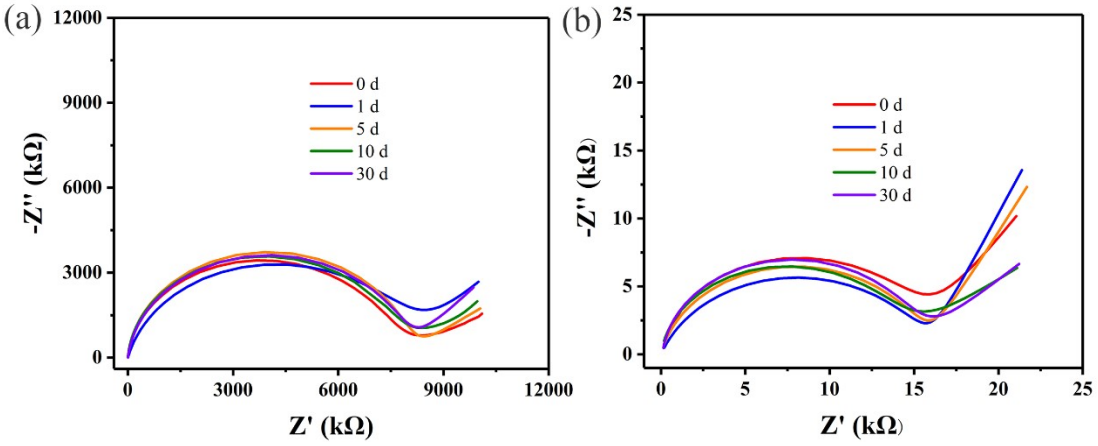

References

1 D. Guo, Y. Z. Zhuo, A. N. Lai, Q. G. Zhang, A. M. Zhu and Q. L. Liu, *J. Membr. Sci.*, 2016, **518**, 295-304.

2 M. Talu, E. U. Demiroglu, S. Yurdakul and S. Badoglu, *Spectrochim. Acta. A Mol. Biomol. Spectrosc.*, 2015, **134**, 267-275.

3 M. J. Frisch, G. W. Trucks, H. B. Schlegel, G. E. Scuseria, M. A. Robb, J. R. Cheeseman, G. Scalmani, V. Barone, B. Mennucci, G. A. Petersson, H. Nakatsuji, M. Caricato, X. Li, H. P. Hratchian, A. F. Izmaylov, J. Bloino, G. Zheng, J. L. Sonnenberg, M. Hada, M. Ehara, K. Toyota, R. Fukuda, J. Hasegawa, M. Ishida, T. Nakajima, Y. Honda, O. Kitao, H. Nakai, T. Vreven, J. A. Montgomery, J. E. P. Jr., F. Ogliaro, M. Bearpark, J. J. Heyd, E. Brothers, K. N. Kudin, V. N. Staroverov, R. Kobayashi, J. Normand, K. Raghavachari, A. Rendell, J. C. Burant, S. S. Iyengar, J. Tomasi, M. Cossi, N. Rega, J. M. Millam, M. Klene, J. E. Knox, J. B. Cross, V. Bakken, C. Adamo, J. Jaramillo, R. Gomperts, R. E. Stratmann, O. Yazyev, A. J. Austin, R. Cammi, C. Pomelli, J. W. Ochterski, R. L. Martin, K. Morokuma, V. G. Zakrzewski, G. A. Voth, P. Salvador, J. J. Dannenberg, S. Dapprich, A. D. Daniels, O. Farkas, J. B. Foresman, J. V. Ortiz, J. Cioslowski and D. J. Fox, Gaussian 09, Revision D.01. Gaussian, Inc.: Wallingford, CT, 2013.

4 P. A. Provencher and J. A. Love, *J. Org. Chem.*, 2015, **80**, 9603-9609.

5 P. Tang, H. T. Leung and G. Sun, *Anal. Chem.*, 2018, **90**, 14593-14601.

6 P. Tang, N. T. Nguyen, J. G. Lo and G. Sun, *ACS Appl. Mater. Interfaces*, 2019, **11**, 13632-13641.

7 W. Yin, H. Li, A. S. R. Chesman, B. Tadgell, A. D. Scully, M. Wang, W. Huang, C. R. McNeill, W. W. H. Wong, N. V. Medhekar, P. Mulvaney and J. J. Jasieniak, *ACS Nano*, 2021, **15**, 1454-1464.

8 W. Chen, S. A. Elfeky, Y. Nonne, L. Male, K. Ahmed, C. Amiable, P. Axe, S. Yamada, T. D. James, S. D. Bull and J. S. Fossey, *Chem. Commun.*, 2011, **47**, 253-255.